The Journal of Experimental Biology 209, 327-342
Published by The Company of Biologists 2006
doi:10.1242/jeb.01982

Neural responses of goldfish lateral line afferents to vortex motions

Boris Phillippe Chagnaud[1,*], Horst Bleckmann[1] and Jacob Engelmann[1,2,*,†]

[1]*Institute for Zoology, University of Bonn, Poppelsdorfer Schloss, 53115 Bonn, Germany and* [2]*Institute Alfred Fessard, Centre National de la Recherche Scientifique, 91198 Gif sur Yvette, France*

*Authors contributed equally to this research

†Author for correspondence (e-mail: jacob.engelmann@uni-bonn.de)

Accepted 11 November 2005

Summary

The lateral line system of fish is sensitive to weak water motions. We recorded from posterior lateral line nerve afferents while stimulating goldfish, *Carassius auratus*, with unidirectional water flow and with a vortex ring. Posterior lateral line afferents of goldfish were either flow sensitive or flow insensitive. Both types of afferents responded to a vortex ring that passed the fish laterally with one to three reproducible patterns of neural activity, followed by activity patterns that were less reproducible. Using particle image velocimetry, we visualized and quantified the water motions in the vertical plane next to the surface of the fish while recording from lateral line afferents. Early response components correlated with the direction of water motions that occurred at the position of the neuromast recorded from. By contrast, neural activity that occurred after the vortex had passed the fish barely predicted the direction of water motions. These results are in agreement with the known directional sensitivity of hair cells and indicate that fish might be able to extract sensory information from complex stimuli like vortices by comparing the activity of a whole array of neuromasts. The stimulus used in this study is novel to lateral line research and resembles some of the hydrodynamic stimuli that fish might encounter in their natural environments. We expect that by combining naturalistic hydrodynamic stimuli and central nervous recordings, we will learn if and how hydrodynamic feature detection is accomplished by the lateral line system.

Supplementary material available online at
http://jeb.biologists.org/cgi/content/full/209/2/327/DC1

Key words: posterior lateral line, particle image velocimetry, teleost fish, *Carassius auratus*.

Introduction

Fishes and aquatic amphibians use the mechanosensory lateral line to detect weak water motions such as those generated by conspecifics, predators or prey (Bleckmann, 1994). The smallest functional unit of the lateral line is the neuromast, a sensory structure that consists of hair cells whose ciliary bundles project into a gelatinous cupula. Lateral line neuromasts occur freestanding on the skin (superficial neuromasts) and in lateral line canals (canal neuromasts). Whereas superficial neuromasts are sensitive to water velocity, canal neuromasts respond to the acceleration of the water (Kalmijn, 1988). Lateral line neuromasts contain two populations of hair cells that are antagonistically orientated (Flock and Duvall, 1965; Flock and Wersäll, 1962a). A single afferent may innervate multiple hair cells, all of the same orientation (Münz, 1979).

Vortex motions are one type of natural hydrodynamic stimuli. They occur, for instance, behind inanimate objects exposed to water currents (Vogel, 1994). Trout make use of vortex motions for station holding (Sutterlin and Waddy, 1975) and for the reduction of the costs of locomotion (Liao et al., 2003). Vortex motions are also caused by undulatory swimming fish (Blickhan et al., 1992; Cheng and Chahine, 2001; Drucker and Lauder, 1999; Linden and Turner, 2004). For piscivorous animals, vortex motions may be important for prey detection and hydrodynamic trail following (Hanke and Bleckmann, 2004; Hanke et al., 2000). Seals (Dehnhardt et al., 2001) and some fish (Pohlmann et al., 2004; Pohlmann et al., 2001) most likely use vortex information to track down prey.

We investigated how posterior lateral line nerve (PLLN) fibers responded to a vortex ring that passed the fish laterally. During stimulation, we visualized and quantified the water motions that occurred across the surface of the fish's body with particle image velocimetry (PIV). We found that afferents of the PLLN of the goldfish, *Carassius auratus*, respond to vortex motions with reproducible changes in discharge rate followed by less reproducible, long-lasting changes in neural activity. Early response components correlated with the direction of water motions that occurred at the position of the neuromast recorded from. By contrast, neural activity that occurred after the vortex ring had passed the fish barely predicted the local direction of water motions.

Materials and methods

For the experiments, we purchased 18 goldfish (*Carassius auratus* L.) from a local dealer. Fish (snout–tail length 6.9–9.2 cm) were held in 250 liter aquaria with a 12 h:12 h light:dark cycle. After surgery, fish were transferred to a flow tank (for details, see Engelmann et al., 2002) positioned on a vibration-isolated table (TMC, LINOS Photomics GmbH, Göttinghen, Germany) and fixed in a stainless steel holder. For artificial respiration, a tube was inserted into the fish's mouth. To prevent lateral movements of the fish, a cord was attached to its tailfin and taped to the tank wall. A plastic cylinder, glued on the head of the fish, prevented water from entering the brain cavity and allowed a complete submersion of the fish (the distance between the water surface and the dorsal fin of the fish was at least 1 cm).

Stimulation

We stimulated the lateral line with a sphere (diameter 6 mm) that was attached with a stainless steel shaft (length 11 cm, diameter 0.2 cm) to a Ling vibrator (Model V101; Peabody, MA, USA). Sine waves (50 Hz, 100 ms rise/fall time, duration 1 s) were generated (Superscope II; Somerville, MA, USA) and transferred *via* an A/D converter (MacAdios, Somerville, MA, USA) to a custom-made dB-attenuator whose output was fed into a power amplifier (PA 25; ELDS, Royston, England) that drove the vibrator. The displacement amplitude of the sphere, calibrated in air with a microscope (Laborlux K; Leitz, Leica, Bensheim, Germany), was varied between 1 and 100 μm.

If a nerve fiber was encountered that was sensitive to water motions, the location of the vibrating sphere was slowly changed along the *x*-axis (along the fish's body). This was done manually by moving a sliding plate to which the vibrator was mounted. While moving, the position of the sphere along the length of the fish (*x*-position) changed, whereas its distance (*z*-position) and its elevation (*y*-position) remained constant (cf. Fig. 1). The *x*-position where the vibrating sphere appeared to elicit the strongest response was assumed to be the rostro-caudal position of the neuromast recorded from (hereafter referred to as neuromast). The receptive fields of 25 nerve fibers, in addition, were precisely determined off-line. Receptive field organization was used to determine the exact position and orientation of the neuromast. Since the vibration axis of the sphere was always parallel to the rostro-caudal axis of the fish, afferents that innervate neuromasts with dorso-ventrally oriented hair cells should have biphasic (two peaks of excitation separated by a 180° phase shift) response patterns if the sphere moves along the side of the fish. By contrast, tri-phasic response patterns (three peaks of excitation separated by two 180° phase shifts) should be generated by afferents that innervate neuromasts with horizontally (rostro-caudally) oriented hair cells (Coombs et al., 1996). The phase of the stimulus to which lateral line afferents couple differs by 180° for biphasic responses, while the responses of tri-phasic afferents show two consecutive phase changes of 180° each. From the physics of the flow field of the dipole stimulus it can be concluded that the neuromast innervated by an afferent with a biphasic receptive field is situated at the position where the phase shift occurs; likewise, the position of a neuromast innervated by an afferent with a tri-phasic response is situated in-between the position where the two phase shifts occur (Coombs et al., 1996).

Vortex rings were generated with water pulses pushed by gravity through a 1 ml pipette (tip opening diameter 1 mm). The pipette was connected with a reservoir that rested 1 m above the experimental tank. Pulse onset and pulse duration were controlled with a valve bank (ValveBank 8; Automate Scientific Inc., San Francisco, CA, USA) *via* a computer and the software Superscope II. In most experiments, the tip of the pipette was placed 5 cm rostral to the position of the neuromast (*x*-axis), at the height of the fish's trunk lateral line canal (*y*-axis). If not otherwise stated, the lateral distance between the pipette tip and the fish was 0.5 cm (*z*-axis). For each stimulus condition, stimuli were repeated 7–10 times, with an inter-stimulus interval of 6–12 s.

If a unit that responded to a passing vortex ring could be held long enough, it was also tested for flow sensitivity. Water flow was generated with a propeller (Schottelantrieb 100; Aeronaut, Wernberg-Köblitz, Germany) coupled to a DC motor (Conrad Electronic, Wernberg-Köblitz, Germany) that was driven by a power supply (DIGI 35; Voltcraft, Conrad Electronic, Wernberg-Köblitz, Germany). Water velocity, measured with an anemometer (CTA 90C10; Dantec, Skovlunde, Denmark), was adjusted to 10±0.5 cm s^{-1}. All fish were positioned with their heads towards the flow.

Recordings

We used KCl (3 mol l^{-1})-filled glass microelectrodes (impedance 50–150 MΩ) to record single unit activity from PLLN fibers. Unit activity was amplified (VF 180 Micro Electrode Amplifier; Biologic, Micro Electrode Amplifier, Echirolles, France; bandpass 0–1 kHz and 50 Hz notch-filter), displayed on an oscilloscope (DL1300A; Yokogawa, Amersfoort, The Netherlands) and stored on a DAT-recorder (Dtr 1802, Biologic) for off-line analysis.

Data analysis

Stored responses were high-pass filtered (3 Hz) and fed through a window discriminator (Model 121; WPI, Sarasota, FL, USA) that delivered a square pulse for each action potential. These pulses were digitised by an A/D converter (MacAdios; 12 bit, sampling rate 2 kHz) and stored on disk. Data analysis was carried out with customized scripts in Igor Pro 3.15 (Wavemetrics Inc., Lake Oswego, OR, USA) or MatLab (The MathWorks Cooperation, Natick, MA, USA). Peri-stimulus–time histograms (PSTH) and raster plots were computed to analyze afferent responses that were classified by criteria described in the Results.

Particle image velocimetry (PIV)

A custom-made PIV system was used to visualize and quantify water motions. Neutrally buoyant particles

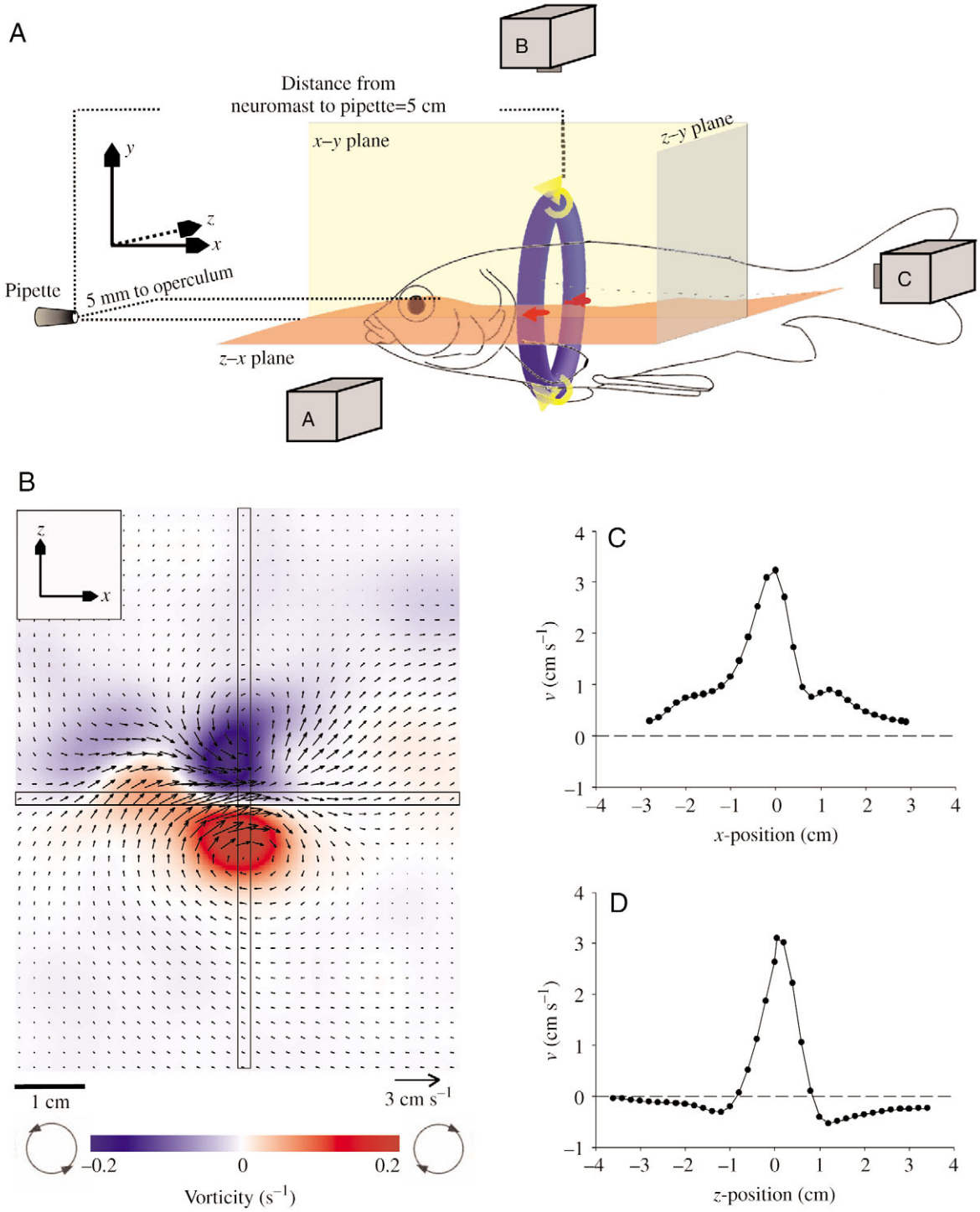

Fig. 1. (A) Schematic drawing of the experimental set-up, a goldfish and a vortex ring. The pipette tip used to generate the vortex is at the left. The elevation of the pipette (*y*-axis) was always at the height of the fish's trunk lateral line canal. The rostro-caudal distance (*x*-axis) between the pipette tip and the neuromast was adjusted to 5 cm. The lateral distance (*z*-axis) of the pipette tip to the operculum of the fish was 0.5 cm, if not stated otherwise. A laser sheet was used to illuminate the particles added to the water. In all cases in which we obtained PIV data and neuronal data, the laser sheet illuminated the *x*–*y* plane (yellow), i.e. a plane that was perpendicular to the fish's rostro-caudal axis. The *x*–*y* plane was placed as close to the skin as possible. For a further characterization of the water motions caused by a vortex ring, the laser sheet was also positioned in the *z*–*x* plane (red) or in the *z*–*y* plane (gray). (B) Vectors (arrows) and vorticity (blue, counterclockwise; red, clockwise) of the particle motions recorded 400 ms after valve opening measured in the horizontal (*z*–*x*) plane (see A) in the absence of a fish. (C,D) Velocities (*v*) directed parallel to the *x*-axis, calculated from the vectors highlighted by the longitudinal boxes in B. The plot in C transects the vortex through its midline and reveals the central flow. The plot in D transects the laser sheet in the *z*-axis. Here, the central flow is bordered by two vortex cores of minimal velocity and a region where the flow direction is opposite to the jet flow. The diameter of the vortex ring is approximately 3 cm.

(Vestosint 1101, Hüls, Berlin, Germany) – suspended in the water – were illuminated with a 1 mm-thick light sheet that was generated with a constant wave laser pointer (Schwäbisch Gmünd; HB Components, Schwäbisch Gmünd, Germany). If not otherwise stated, the light sheet was in a vertical (*x*–*y*) plane, oriented parallel to the lateral surface of the fish (see Fig. 1A). Due to the curvature of the fish's body, the distance between the light sheet and the fish varied between 1 mm (minimal distance) and 3 mm. The illuminated particles were filmed with a CCD camera (DMK 803; frame rate 25 Hz; The Imagingsource, Bremen, Germany) and stored on a video recorder (EV-S9000E Pal; Sony, Tokyo, Japan) together with the electrophysiological data and the trigger used to open the valve. Videos were digitised (DC 30; MiroVideo, Pinnacles System, Mountain View, CA, USA), stored on disk and converted to avi-movies (Premiere 6.0; Adobe Systems, Mountain View, CA, USA).

Individual pictures were taken with an exposure time of 1/250 ms at a frame rate of 25 Hz, i.e. the temporal precision of the PIV analysis was ⩾40 ms. For the construction of PIV-images, movies of particle motions were imported frame by frame in Davis 7 (LaVision, Göttingen, Germany), and successive frames were analyzed by a time-series sequential cross-correlation. The interrogation window size for this cross-correlation was 64×64 pixels. To improve the analysis, an overlap among neighboring interrogation windows was applied, which resulted in a window size of 32×32 pixels. Application of a multi-pass filter further reduced the error of the calculated vectors. This filter executed iterative (N=2) evaluations of the same pair of images. In the first pass, a vector was computed and used as a reference for the following pass. In the second pass, the interrogation window of the first frame was shifted by half the amount of the reference vector and in the opposite direction while the interrogation window of the second frame was shifted in the direction by half of the amount of the reference vector. Thus, the correlation in the second pass anticipates the main motion direction of the particles and adjusts the interrogation area such that the maximum number of particles is included. This enhances the precision of the PIV. Finally, a median filter was used to compute the median vector for eight neighboring interrogation windows. If the center vector (surrounded by the eight interrogation windows) differed by >3× root-mean-square from the median vector, the center vector was replaced by the averaged vector obtained from the neighboring interrogation windows. After this computation, the vector plots were post-processed. We used the same median filter and smoothing as during the computation of the vector plots.

Neural responses to a vortex ring were correlated with the water motions. To do so, 5–10 PIV images were averaged and compared with the PSTHs of the respective neural responses. Some afferents continued to fire reproducible bursts after a vortex ring had passed the fish. To find out whether these bursts correlated with hydrodynamic events, vector plots of the particle motions recorded immediately before and during a certain burst were compared. The same procedure was applied to afferents that displayed late non-reproducible bursts. Fast Fourier transformations (FFTs) of the discharge rates of individual units were calculated and compared with the FFTs of the corresponding water motions.

Vector plots

Local flow-direction was obtained from vector orientation. The direction of a vector pointing from rostral to caudal was defined as 0°, while that of a vector pointing in the opposite direction was ±180°. Vectors pointing in a dorsal direction were given a positive sign (0° to +180°), while those pointing in a ventral direction were given a negative sign (0° to –180°). Thus, vector angles less than 90° and greater than –90° indicated water motions in the head-to-tail direction, while those greater than 90° and less than –90° indicated water motions in the tail-to-head direction. In all measurements in which PIV data and neuronal data were simultaneously recorded, the laser sheet was oriented in a vertical plane parallel to the fish.

Stimulus measurements

In addition to the PIV analysis, water velocities were measured with a constant temperature anemometer (CTA 90C10; Dantec, Scovlunde, Denmark). Compared with PIV data based on a low frame rate (25 Hz), anemometer measurements have a higher temporal resolution. We calibrated the anemometer by moving its probe, attached to a motor-driven arm, with a defined speed through the experimental tank (10 trials/speed). During measurements, the orientation of the sensitive element (wire) of the anemometer was vertical. The wire was positioned 1–2 mm lateral (z-axis) from the fish and 5 cm away (x-axis) from the tip of the pipette that generated the vortex rings. During anemometer measurements, a fish was positioned in the flow tank. The pressure components of a vortex ring stimulus were measured with a hydrophone (type 8103; Brüel & Kjaer, Nærum, Denmark), placed at the same position as the probe of the anemometer (Fig. 3A).

Results

Physical properties of the vortex stimulus

In all experiments, we stimulated the lateral line with a vortex ring that passed the fish laterally from anterior to posterior. Fig. 1A shows the scheme of this vortex and the three planes used to monitor particle motions. An example for the vortex ring-caused particle motions in the horizontal (red) plane is shown in Fig. 1B. The vector plot in Fig. 1B depicts two vortex cores that rotate in opposite directions and that are separated by a central flow (Fig. 1C). This central flow moves parallel to the x-axis (maximal flow speed that could be detected with our PIV settings was 5 cm s^{-1}). Five centimeters away from the pipette tip (in the x-direction), the vortex cores (regions of zero velocity) are separated by approximately 2 cm. The complete vortex ring had a diameter of approximately

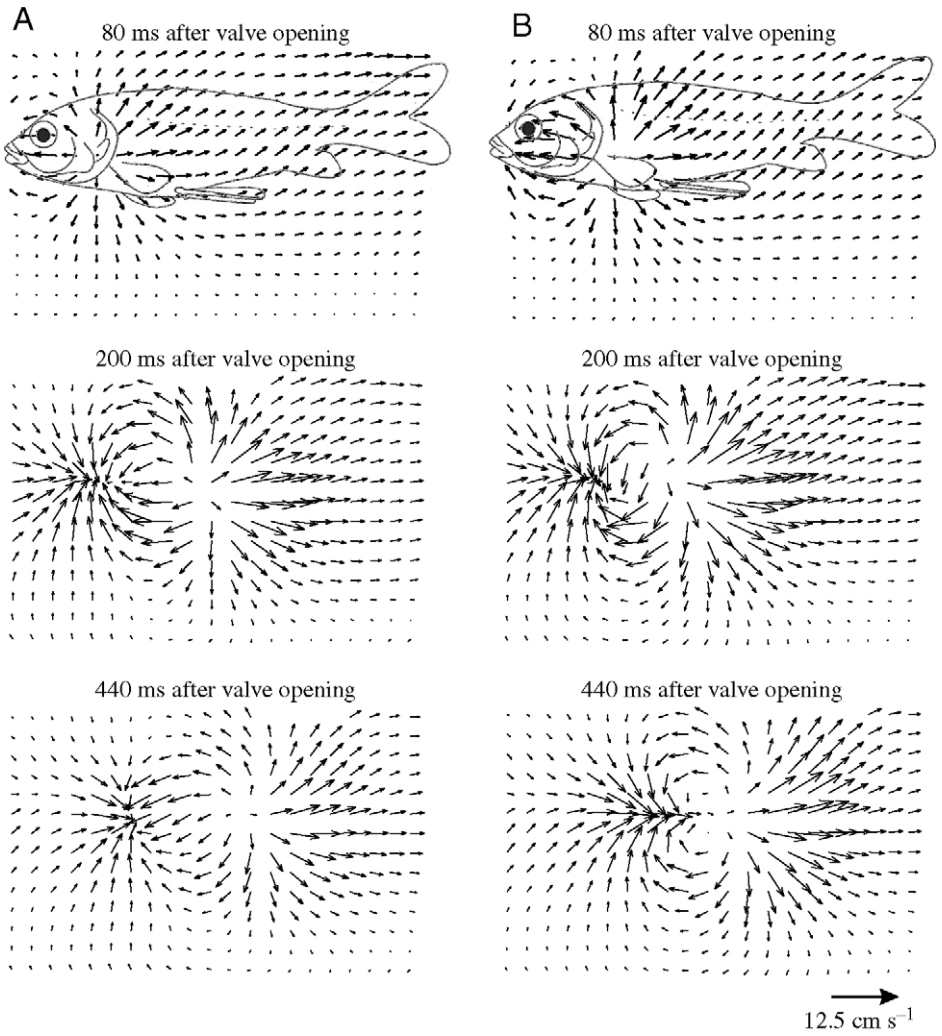

Fig. 2. Vector plots of particle motions in the vertical plane recorded 80 ms (top), 200 ms (middle) and 440 ms (bottom) after valve opening. Vector plots are based on (A) individual and (B) averaged trials (n=9). Arrows indicate the direction and velocity of particle motions. Note that the averaged plots are similar to the plots based on individual trials, i.e. that the vortex stimulus was reproducible from trial to trial. Scale vector, 12.5 cm s^{-1}. In this figure, as well as in Figs 7–9, 11, 12, the fish schematic indicates the size, location and orientation of the fish relative to the vector plots.

3 cm (Fig. 1D). Imaging the stimulus in the horizontal (x–z) plane (Fig. 1) and in a vertical (x–y) plane that was parallel to the fish (Fig. 2) revealed that the unidirectional water flow generated by the pipette resulted in the formation of a vortex ring at a distance approximately 3.5 cm away from the pipette tip. Fig. 2 shows the vertical particle motions (yellow plane in Fig. 1A) caused by the vortex ring as it passes the fish laterally (see supplementary material). Note that the particle motions surrounding the jet flow are nearly symmetrical with respect to the x-axis. PIV images based on single trials (Fig. 2A) were similar to the PIV images based on averaged trials (Fig. 2B), i.e. the stimulus was reproducible from trial to trial.

In some cases, we aligned the laser sheet perpendicular to the lateral surface of the fish (y–z plane in Fig. 1A). In these cases, the distance (x-axis) between the pipette tip and the laser sheet was adjusted to 5 cm, i.e. to the same distance as the neuromast in the physiological experiments. The above alignment was chosen to determine the times at which distinct phases of the vortex ring passed the neuromast (see below). The PIV measurements (Fig. 3A) show that the first water motions caused by the vortex ring reached the laser sheet about 160–200 ms after valve opening. These measurements – obtained without a fish being present – confirmed that particle motions were directed radially around the jet flow. This radial flow, which represents the opening of the vortex ring, lasted for ~120 ms (from 160 ms to 280 ms; Fig. 3A). Following this opening, a symmetrical reversion of flow direction, i.e. the closure of the vortex ring, started (time 400–520 ms). During this closure, particles moved towards the jet flow. Thereafter, another reversal in flow direction occurred (not shown).

Hydrophone recordings, done simultaneously with the PIV measurements, revealed that the vortex ring also caused high-frequency pressure pulses. At peak pressure (Fig. 3B), which was associated with maximum flow velocity (Fig. 3C), the vortex ring reached the laser sheet. After the high-frequency pressure pulses, a less defined large drop in hydrodynamic pressure occurred, which reached its minimum 1600 ms after valve opening. The edge of the hydrophone was placed at the same x- and z-distance from the pipette as the neuromast in the physiological experiments. Thus, the hydrophone interfered with the water motions of the vortex ring. It is noteworthy that the vector pattern remained fairly symmetrical and that the edge of the hydrophone did not reach the central jet flow (Fig. 3A).

Based on anemometer measurements (Fig. 3C), the first changes in flow velocity occurred after 160–180 ms; peak water velocities could be measured after 250–270 ms. Thereafter, water velocity declined, and 6 s after valve opening water motions were no longer detectable. Both anemometer and hydrophone measurements (see small s.d. of graphs in Fig. 3B,C) confirmed that the stimulus was reproducible from trial to trial. In contrast to water (particle) motions, pressure changes were less reproducible.

The reproducibility of the particle (water) motions was also evident when we calculated all particle velocities obtained from a single vertical row of integration windows. In such a row, particle (water) velocities in individual trials were indistinguishable from those based on averaged trials [40 ms before valve opening, the mean water velocity (vector length) was 1.2 cm s^{-1} (single trial) and 1.1 cm s^{-1} (averaged trials) (Wilcoxon test, Z=–1.376, P=0.169); 200 ms after valve opening, the mean particle (water) velocity (vector length) was 3.4 cm s^{-1} (single trial) and 3.0 cm s^{-1} (averaged trials) (Wilcoxon test, Z=–1.07, P=0.285)].

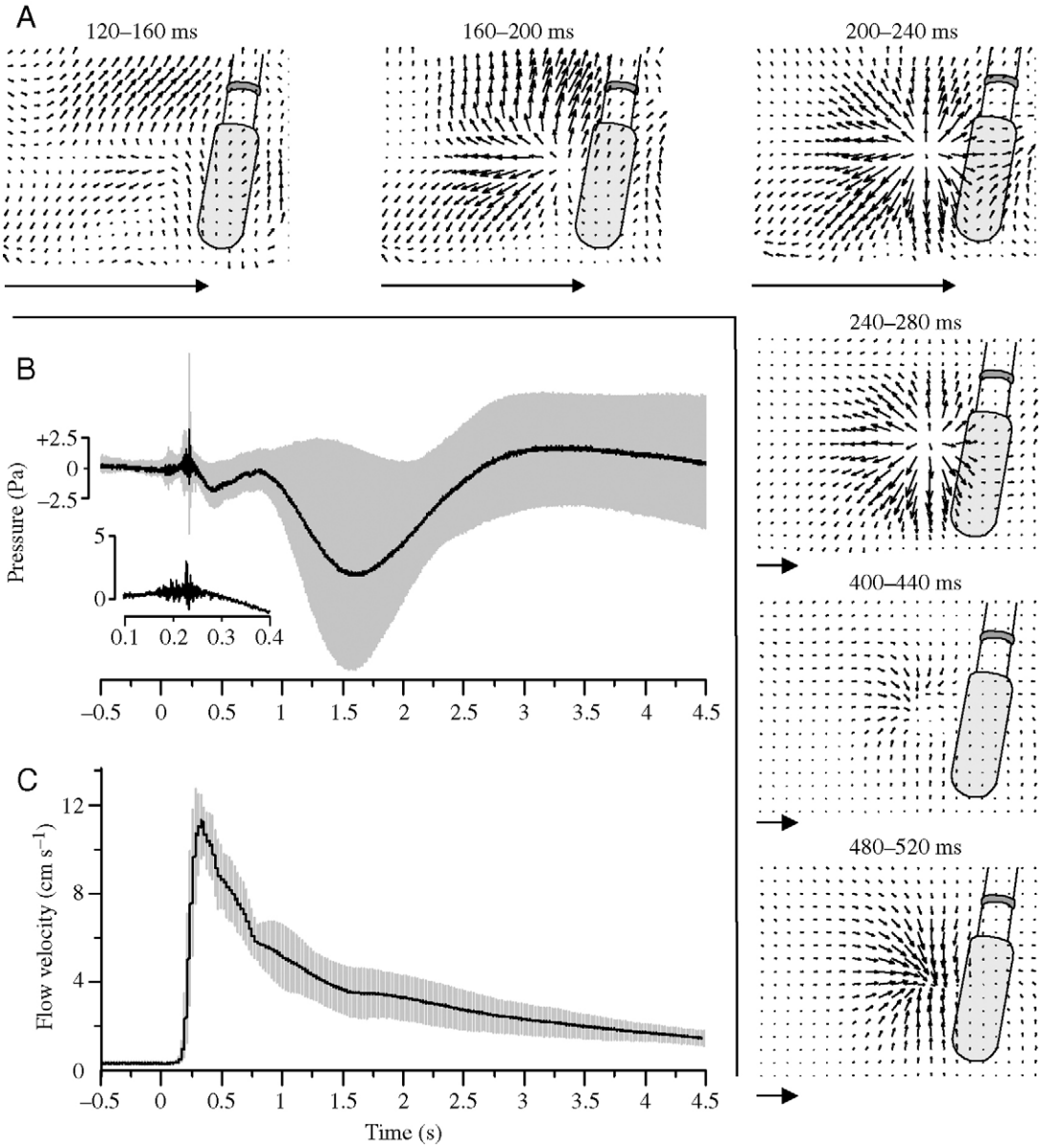

Fig. 3. (A) Averaged (n=10) vector plots based on particle motions recorded after valve opening at the times indicated. The orientation of the laser sheet was orthogonal to the propagation direction of the stimulus (z–y plane in Fig. 1A). The distance between the pipette and the laser sheet was adjusted to 5 cm. Scaling vectors (large horizontal arrows) represent 12.5 cm s^{-1}. For better visualization, the vectors are enlarged in the first three images. For parallel pressure measurements, a hydrophone was placed 5 cm away from the pipette tip. (B) Mean changes in hydrodynamic pressure (n=10) caused by the vortex ring. Inset: pressure changes, measured 100–400 ms after valve opening, at an expanded time scale. (C) Mean water velocity (n=10) measured with an anemometer. In B and C, zero indicates the time of valve opening. Gray shaded areas in B and C represent ±1 s.d.

Forty milliseconds before valve opening, the orientation of vectors based on single trials (mean=56°) differed from the orientation of vectors based on averaged trials (mean=62°; Wilcoxon test, Z =–2.395, P=0.01). By contrast, 200 ms after valve opening, vector orientations based on single trials (mean=–59°) were indistinguishable from vector orientations based on averaged trials (mean=40°; Wilcoxon test, Z=–1.478, P=0.14). Thus, both vector length (particle velocities) and vector orientation (direction of particle motion) were reproducible from trial to trial. However, it should be mentioned that in the physiological experiments the vortex ring stimulus was altered by the presence of the fish. This was especially true in the experiments in which the lateral distance between the pipette tip and the fish was only 0.5 cm. However, as will be detailed below, the discharge patterns of the primary lateral line afferents evoked by the vortex stimulus remained fairly constant up to the lateral distance of 3.5 cm of the pipette tip. Therefore, the presence of the fish cannot have altered the vortex ring stimulus completely. Nevertheless, in the following, we prefer the term 'vortex stimulus' instead of vortex ring stimulus.

Physiology

Single unit recordings were made from 96 afferents in the left (ipsilateral) PLLN of 18 goldfish. Seventy-three afferents responded to water motions; the remaining 23 afferents did not respond to the stimulus and were discarded from further analysis. The ongoing activity of all afferents that responded to water motions was determined, and the responses of these afferents to vortex stimuli [N (total number of fish) = 16; n (total number of cells) = 69] were investigated. If possible, we also investigated the responses of these afferents (N=14; n=41) to unidirectional water flow (10 cm s^{-1}). Twenty-six (63%) afferents significantly increased their discharge rate if exposed to unidirectional water flow (Wilcoxon test, $P \leqslant 0.01$) and were thus classified as type I afferents (Engelmann et al., 2000). The remaining 15 afferents (37%) were insensitive to unidirectional water flow (Wilcoxon test, $P \geqslant 0.01$) and were thus classified as type II afferents (Engelmann et al., 2000). Ongoing activity of type I afferents (19.3±10.6 spikes s^{-1}) was not significantly different from the ongoing activity of type II afferents (18.7±14.9 spikes s^{-1}; Mann–Whitney U-test, U=181; Z=–0.379, P=0.72).

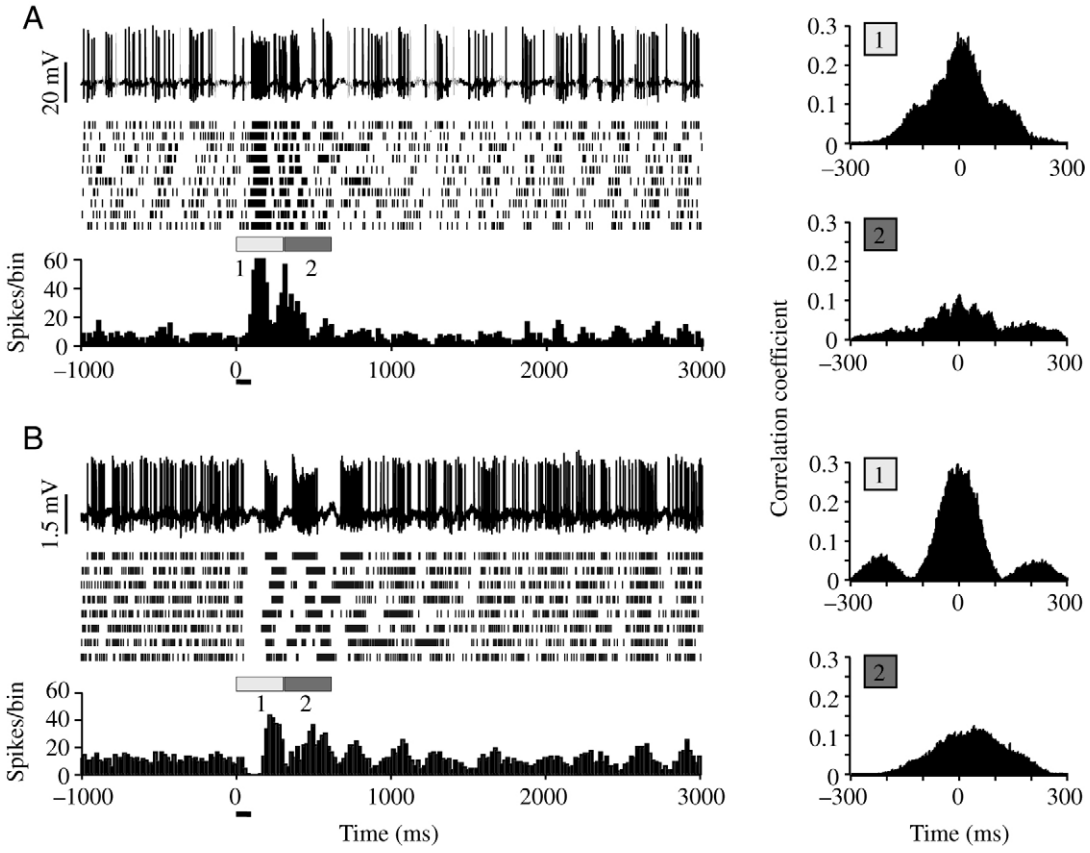

Fig. 4. Discharge patterns of goldfish posterior lateral line nerve (PLLN)-afferents to the vortex stimulus passing the fish laterally from anterior to posterior. Afferents responded with an initial increase (E-afferents, A) or decrease in discharge rate (I-afferents, B). In A and B, raster plots of the responses to 10 (A) and 8 (B) stimulus presentations and their corresponding peri-stimulus–time histograms (PSTHs; binwidth 20 ms) are shown. Top traces in A and B show original recordings that correspond to the respective first trace in the raster plots. Horizontal bars below the PSTHs indicate the time of valve opening. The initial response components were fairly reproducible from trial to trial. This was quantified by calculating the correlation coefficients between individual trials (n=5) for the first (A and B, top right) and second (A and B, bottom right) 300 ms following valve opening.

Table 1. *Response parameters of E- and I-afferents*

	E-afferents* (*n*=34)	I-afferents* (*n*=24)	Mann–Whitney *U*-test	
			Z	*P*
Initial response latency (ms)	117±74 (20–410)	128±44 (42–240)	–1.603	0.11
Initial response duration (ms)	119±68 (88–497)	69±32 (40–149)	–3.13	0.0017
Total response duration (ms)	862±859 (155–3465)	2060±3053(170–9768)	–2.08	0.037
Peak total response (spikes/bin)	31±14 (7–67)	35±14 (13–64)	–1.20	0.229
Latency of peak (ms)	187±83 (82–460)	323±101 (160–567)	–4.634	<0.0001

Values are means ± s.d. (range).

Afferent responses to vortex motions

If not otherwise stated, the distance between the pipette tip and the neuromast recorded from (hereafter simply called neuromast) was adjusted to 5 cm (distance along the *x*-axis) and 0.5 cm (distance along the *z*-axis), respectively. In all cases, the rostro-caudal position of the neuromast was determined on-line. In 18 cases, the position of the neuromast was also determined more precisely off-line (see Materials and methods). Comparing neuromast positions determined on-line with the neuromast positions determined off-line revealed a mean difference of 0.1±1.24 cm (*n*=18).

All (*n*=69) but seven primary afferents responded to a vortex stimulus that passed the fish laterally. Four of the unresponsive afferents also failed to respond to a stationary dipole stimulus (duration 1 s, frequency 50 Hz, peak-to-peak displacement amplitude 100 μm) but responded to water motions caused by a pipette that was moved manually along the side of the fish. The remaining three afferents showed no responses to any of

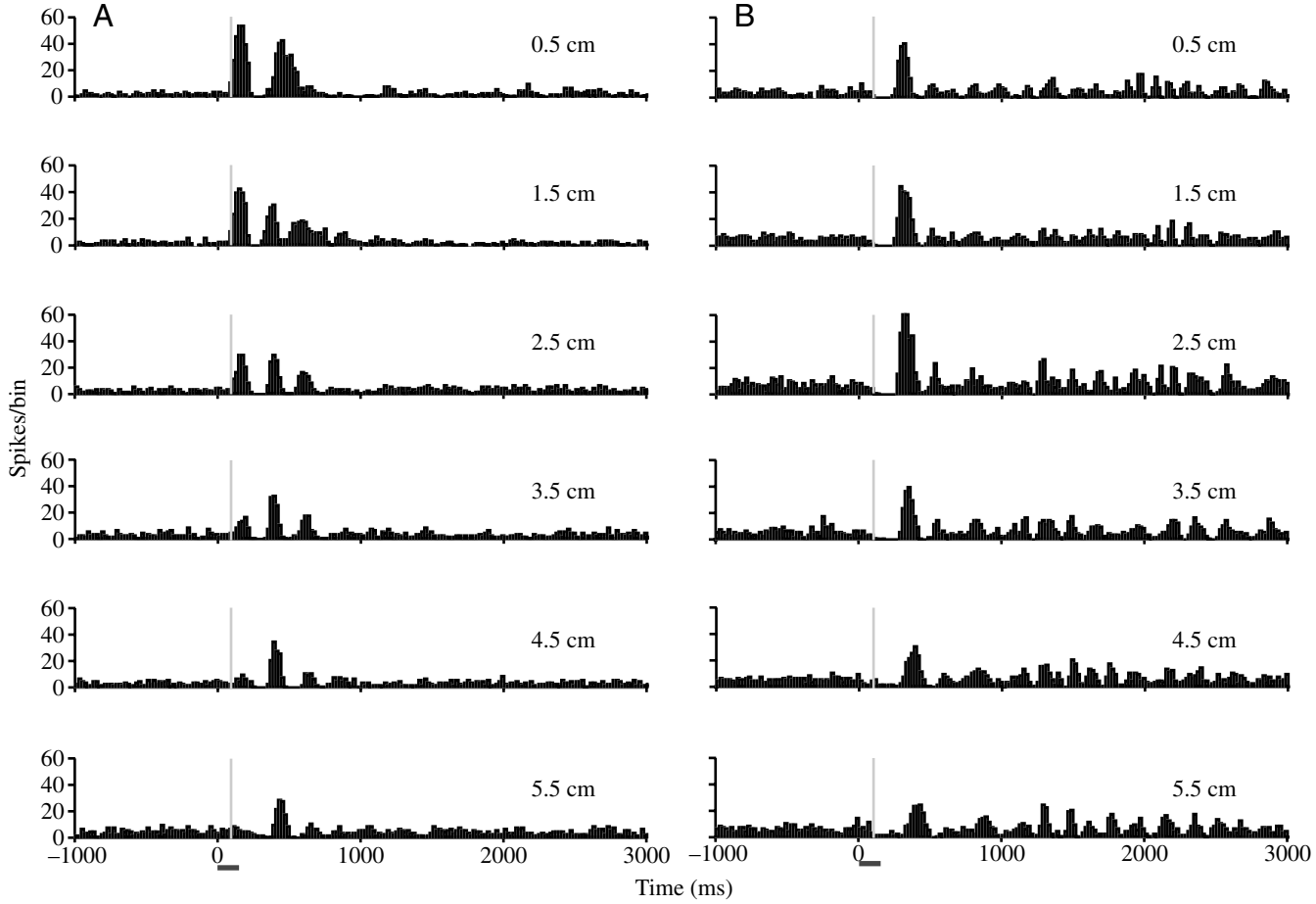

Fig. 5. The responses of an E-afferent (A) and an I-afferent (B) to the vortex stimulus passing the fish laterally at the distances indicated. Each peri-stimulus–time histograms (PSTH) is based on eight trials. Horizontal bars represent time of valve opening. Gray vertical lines indicate the time of response onset of the top traces (lateral distance 0.5 cm).

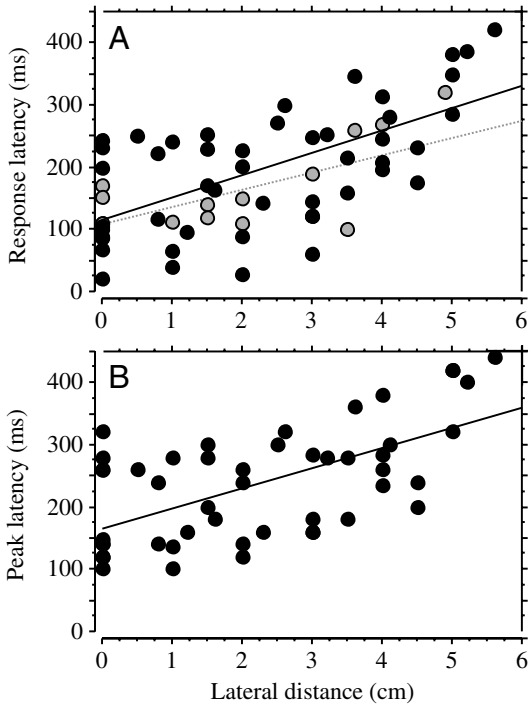

Fig. 6. Response latencies (A) and peak latencies (B) as a function of lateral (*z*-axis) pipette distance. Black circles, E-afferents; gray circles, I-afferents. Note that B contains only E-afferents. Linear regression lines were calculated across the data (E-afferents, solid lines; I-afferents, dotted line). See Results for the equation for each line.

the hydrodynamic stimuli applied. In four afferents that responded to the vortex, even the initial responses were not reproducible across stimulus presentations. Therefore, these afferents were not further investigated. The remaining 58 afferents responded to the vortex with repeatable discharges. Controls (n=12) showed that the responses were caused by water motions and not by electrical or mechanical artifacts caused by valve opening.

Temporal response patterns

Peripheral lateral line units responded with monophasic (n=8), biphasic (n=27) or triphasic (n=23) discharge patterns to the vortex stimulus. Monophasic responses consisted of an increase or a decrease in ongoing activity. Biphasic responses consisted of an increase in ongoing activity followed by a decrease in neural activity or *vice versa*. Triphasic responses contained an additional reproducible increase or decrease in neural activity.

Afferents that responded with an initial increase in discharge rate were classified as E-afferents (n=34; Fig. 4A), while those that responded with an initial decrease in discharge rate were

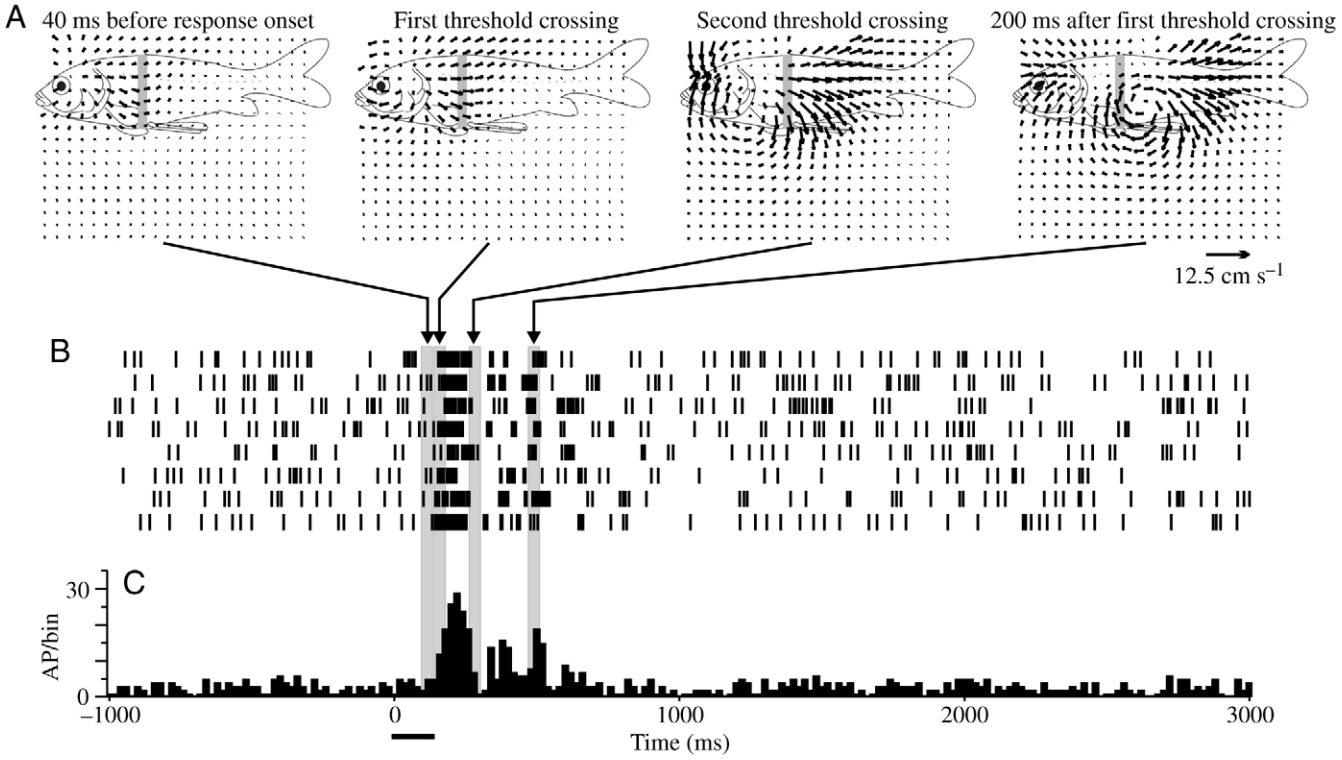

Fig. 7. E-afferent response and PIV. (A) Averaged (n=8) vector plots based on particle motions – measured in the vertical plane – caused by the vortex stimulus. Particle motions were recorded (from left to right) immediately before first threshold crossing, at first and second threshold crossing, and 200 ms after second threshold crossing. Gray bars indicate the rostro-caudal position of the neuromast. (B) Raster plots of the responses to a vortex stimulus and (C) peri-stimulus–time histograms (PSTHs; bin width 20 ms) based on these raster plots. In this figure and in Figs 8, 9, the vertical gray bars indicate the neural activity recorded during the 40 ms time windows on which the respective PIV images are based.

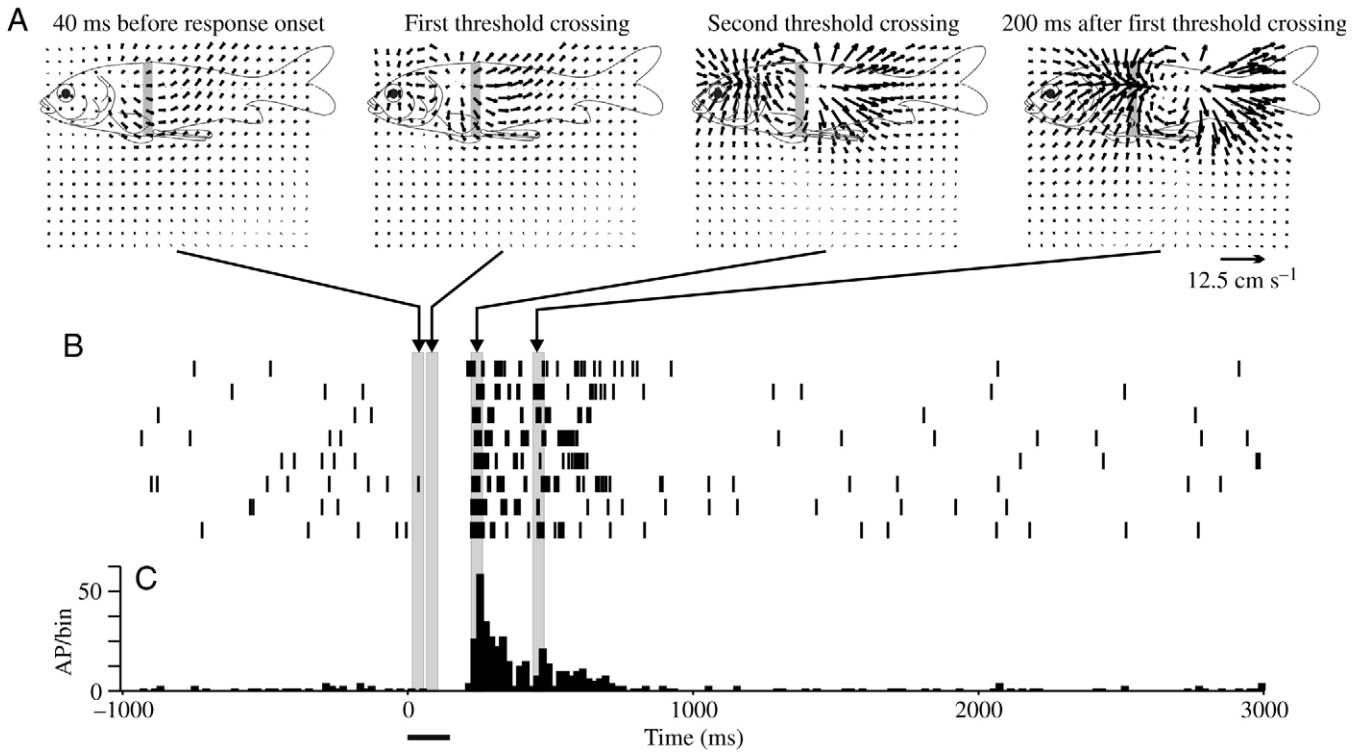

Fig. 8. I-afferent response and PIV. (A) Averaged (n=8) vector plots based on particle motions caused by the vortex stimulus. Particle motions were recorded (from left to right) immediately before first threshold crossing, at first and second threshold crossing, and 200 ms after the second threshold crossing. (B) Raster plots of the responses and (C) peri-stimulus–time histograms (PSTHs; bin width 20 ms) based on these raster plots. See Fig. 7 for further details.

classified as I-afferents (n=24; Fig. 4B). Afferents responded with distinct temporal discharge patterns. To classify these discharge patterns, we analyzed the PSTHs (bin width 20 ms). To be scored as a response, neural activity had to differ from ongoing activity plus/minus three times its standard deviation – measured for 1 s immediately before valve opening – for at least 40 ms. Response duration was defined as the time between first and last threshold crossing. Responses to the vortex stimulus consisted of an initial reproducible component and a late less-reproducible component. The initial reproducible component was characterized by 1–3 predictable changes (increases or decreases; see above) in neural activity. We determined the maximum discharge rate and the latency of the initial response component.

The initial reproducible response component lasted for ~300 ms. PIV data (see below) revealed that the initial response component occurred while the vortex stimulus passed the fish. By contrast, the late response component coincided with the less-reproducible water motions that occurred after the vortex stimulus had passed the neuromast; this was confirmed by calculating the mean cross-correlation coefficient between every pair of five consecutive responses for 12 randomly chosen cells (see cross-correlation data in Fig. 4B, right). Cross-correlation coefficients were 0.10±0.09 (mean ± s.d.) for the 300 ms preceding valve opening (control), 0.32±0.08 for the 300 ms following valve opening and 0.20±0.11 for the next 300 ms following valve opening. Thus, for the time spans selected, reproducibility was highest for the 300 ms directly following valve opening.

The late response component of E- and I-afferents lasted for ~2 s (in four cases for up to 6 s) and consisted of several bursts. As revealed by cross-correlation analysis, the occurrence of these late bursts was usually ill defined, i.e. they occurred at unpredictable times (e.g. Figs 4, 7–9, 12). However, in four afferents, the late bursts were reproducible (e.g. Fig. 11).

With respect to valve opening, E-afferents responded with a latency of 117±74 ms (n=34), I-afferents had a latency of 128±44 ms (n=24). Latencies of E- and I-afferents were not significantly different (Mann–Whitney U-test, U=306.5, Z=–1.603, P=0.11). Maximum discharge rates occurred later in I-afferents than in E-afferents; however, in terms of peak discharge rates, I- and E-afferents were not different (Table 1).

Afferents were or were not sensitive to unidirectional water flow. There was no correlation between flow sensitivity and response type. Out of the 41 afferents tested, 26 were flow sensitive (16 E-afferents, eight I-afferents, two undefined) and 15 were flow insensitive (four E-afferents, six I-afferents, five undefined). Neither response duration (Mann–Whitney U-test, U=111; Z=–0.340, P=0.75; type I afferents, 810.1±823.6 ms; type II afferents, 874.8±659.8 ms) nor the duration of the initial response component (Mann–Whitney U-test, U=110; Z=–0.379, P=0.72; type I afferents, 102.2±68.3 ms; type II afferents, 94.0±67.4 ms) was significantly different in type I and type II afferents.

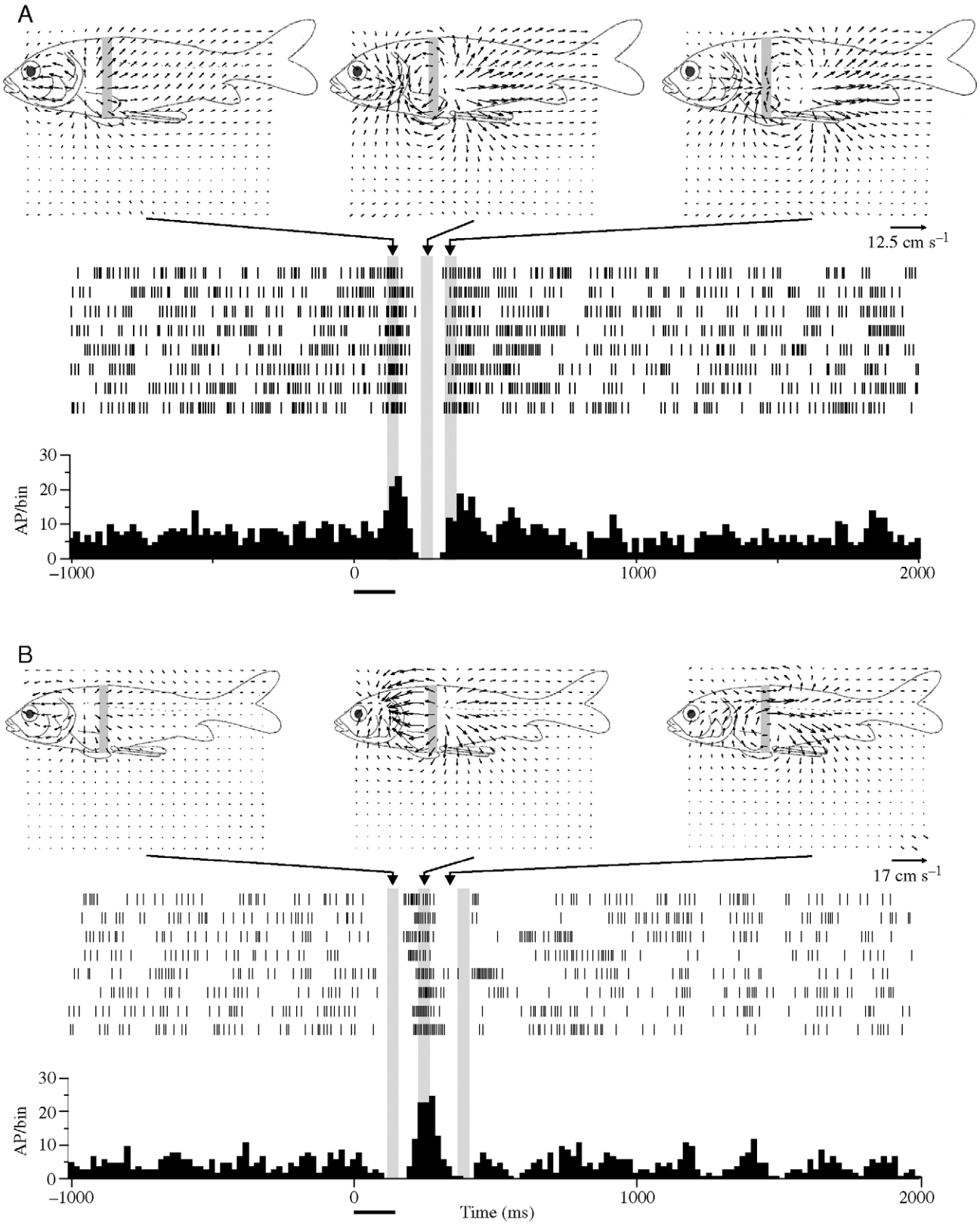

Fig. 9. E-afferent response (A) and I-afferent response (B). (Top) Averaged (n=8) vector plots based on particle motions caused by the vortex stimulus. Particle motions were recorded (from left to right) at first, second and third threshold crossing. (Middle) Raster plots of the responses and (bottom) peri-stimulus–time histograms (PSTHs; bin width 20 ms) based on these raster plots. Note that changes in the initial response components from excitation to inhibition are associated with approximate 180° changes in flow direction at the rostro-caudal level of the neuromasts (gray bars on fish schematic). See Fig. 7 for further details.

Lateral pipette tip distance and afferent responses

Due to the curvature of the fish, the distance between the opening of the pipette tip and the fish was not constant along the length of the fish. Therefore, we investigated the influence of the lateral distance of the pipette tip (distance along the z-axis) on the responses of 10 E- and four I-afferents (test range 0.5–5.5 cm).

Up to a lateral distance of 3.5 cm, the temporal response patterns of lateral line afferents remained fairly constant (Fig. 5A). A linear regression analysis revealed that the latency of the initial response component increased with increasing lateral tip distance (E-afferents, k=114.89+35.89z, r^2=0.39, P<0.01; I-afferents, k=106.93+27.76z, r^2=0.43, P<0.01; Fig. 6A). In E-afferents, both the latency of the first response peak (k=163.42+32.7z, r^2=0.37, P<0.01; Fig. 6B; I-afferents were not investigated) and the latency of the maximum response peak (which may be identical with the first response peak; k=216.1+30.2z, r^2=0.28, P<0.01) also increased with increasing lateral distance of the pipette tip. By contrast, neither the duration of the initial response component nor the duration of the total response changed in E-afferents (duration of the initial response component, d=98.8–6.2z, r^2=0.05, P=0.12; duration of the total response, d=1915.4–82.8z, r^2=0.01, P=0.43) and I-afferents (initial response, d=56.9–1.1z, r^2=0.005, P=0.84; total response, d=1218.4+112.6z, r^2=0.03, P=0.55). In E-afferents, there was no correlation between lateral tip distance and peak amplitude of the first response component (d=28.2–1.6z, r^2=0.039, P=0.18). Thus, with increasing lateral tip distances, afferent responses were increasingly delayed, yet peak response amplitudes and response durations were not altered.

Neural responses and water motions

To investigate the relationship between neural activity and water motions, we correlated PIV data with the neurophysiological data. The vector plots in Figs 7, 8 are based on particle motions recorded 40 ms before response onset, at the first and second crossing of response threshold and 200 ms after the first threshold crossing, i.e. at the time when the ill-defined response component occurred. The responses of an E-afferent to the vortex stimulus are shown in Fig. 7A. At the rostro-caudal position of the neuromast (see gray bars in the fish drawings of Fig. 7A), a water flow from anterior to posterior correlates with an increase in neural activity. After this initial increase in neural activity, flow direction started to reverse. This reversal correlates with a decrease in neural activity, followed by several less reproducible excitatory response components. The responses of an I-afferent are depicted in Fig. 8. At the rostro-caudal position of the neuromast (see gray bars in the fish drawings of Fig. 8A), water flow from anterior to posterior correlates with a decrease in neural activity. After this initial decrease, flow direction reversed. This reversal correlates with a strong increase in neural activity, followed by less reproducible excitatory response components. Thus, the neural responses reflect the directional sensitivity of lateral line afferents (hair cells). The correlation between the direction of particle motions and discharge rates was investigated in greater detail in six afferents that innervated neuromasts whose rostro-caudal positions were precisely determined off-line (see Materials and methods). For the time of the initial increase/decrease and the following decrease/increase in neural activity, we calculated the mean flow (vector) orientation for the PIV column depicted by the gray bar (for an example, see Fig. 9). A change from a decrease to an increase (or *vice versa*) in neural activity was accompanied by a 163.5±15.9° (mean ± s.d.; n=6, Wilcoxon test, P<0.001) change in flow direction. This shows that flow direction reversed between the first and the second initial response component.

In 14 E-afferents, the initial increase in neural activity was followed by a decrease and a second sharp increase in neural activity (for an example, see Fig. 9A). Seven I-afferents showed an inverse behavior, i.e. the initial decrease in neural activity was followed by a sharp increase and another sharp decrease in neural activity (for an example, see Fig. 9B). In 12 of these afferents, we investigated whether the second reversal in neural activity also correlated with a reversal in flow

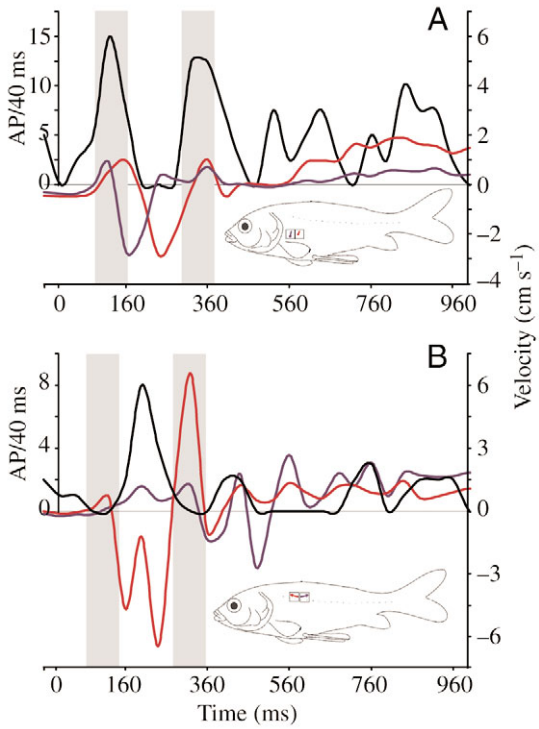

Fig. 10. Flow velocities (red and blue curves) calculated from interrogation windows (see small squares on fish drawings). Interrogation windows with the red vectors were at the position of the neuromast. The interrogation windows with the blue vectors were slightly more rostral (A) or caudal (B), respectively. The black traces in A and B show the discharge rates (spikes/40 ms) obtained in a single trial of the E-afferent (A) and I-afferent (B) whose data are shown in Fig. 9. Negative velocities represent flow in the tail-to-head direction; positive velocities represent flow in the head-to-tail direction. Gray bars indicate the times when the first and third reproducible response components occurred. Zero indicates the time of valve opening.

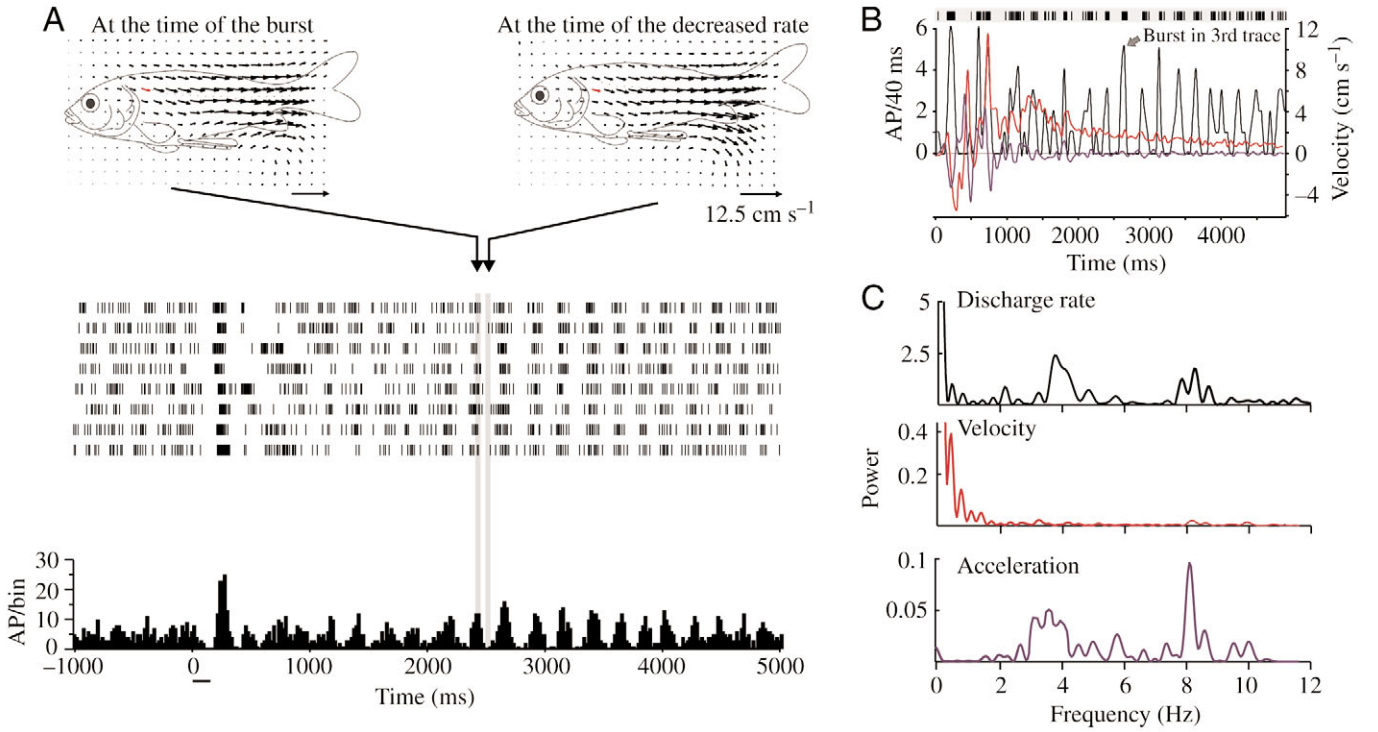

Fig. 11. (A) (Top) Averaged (n=8) vector plots based on particle motions caused by the vortex stimulus passing the fish laterally. Particle motions were recorded during the reproducible bursts marked by the first vertical gray bar and during the following period of decreased neural activity marked by the second vertical gray bar. (Middle) Raster plots of the responses to the vortex stimulus and (bottom) peri-stimulus–time histograms (PSTH; bin width 20 ms) based on these raster plots. Note that the flow pattern during the bursts marked by the first vertical gray bar was similar to the flow pattern that occurred after the bursts (second vertical gray bar). (B) (Top) Raster plot of the third trial shown in A. (Bottom) discharge rate (spikes per 40 ms, black trace) calculated for that trial, and local water velocities (red trace) obtained from the interrogation window indicated by the red vector in A. This interrogation window is at the position of the neuromast. The blue trace shows the first derivative of the velocity data (i.e. water acceleration). Note that during the late bursts, small rhythmic fluctuations occurred in both local water velocity and local water acceleration. (C) (Top) Fast Fourier transformations (FFTs) of the discharge rate (trial 3 in A) and the corresponding FFTs of the velocity (red; middle) and acceleration traces (blue; bottom) shown in B. Note that both neural activity and water acceleration have peaks at 3 and 8 Hz.

direction. The analysis was again limited to afferents that innervated a neuromast whose rostro-caudal position was precisely determined off-line. In the cases exemplified in Fig. 9, weak water jets applied with a small pipette revealed that the neuromasts were situated in the dorsal half of the fish. Again, the initial response component was associated with a flow in head-to-tail direction (Fig. 9). The following decrease or increase in neural activity correlated with a reversal in flow direction. The third reproducible response component (Fig. 9) correlated with a second reversal in flow direction, i.e. with the flow that occurred after the vortex ring had passed the neuromast. Fig. 10 shows the discharge rates (black traces) of these units as a function of time during a single stimulus presentation. In addition, this figure shows the water velocities (blue and red traces) derived from the two interrogation windows depicted in the fish drawings. While the interrogation window with the red vector was located at the position of the neuromast, the interrogation window with the blue vector was located more rostral (cf. Fig. 10A) or more caudal (cf. Fig. 10B). Negative velocities indicate flow in the tail-to-head direction; positive velocities indicate flow in the head-to-tail direction. In both afferents, the initial response components, i.e. the neural activity that occurred during the first 300 ms after valve opening, was correlated with flow direction. Note that during the initial responses the black and red traces are more similar than the black and blue traces. This was confirmed by a linear correlation between the discharge rate (AP/40 ms) and the rectified water velocities measured at the two interrogation windows. The correlation between red vector length and discharge rates was higher (r^2=0.313 in A and r^2=0.275 in B) than the correlation between blue vector length and discharge rates (r^2=0.072 in A and r^2=0.120 in B) for the first 600 ms of the response. When we correlated discharge rates with vector angles, similar results were obtained (r^2=0.33 for the red vector and 0.001 for the blue vector in A, and r^2=0.39 for the red vector and 0.15 for the blue vector in B). Thus, changes in water motions, measured at the position of the neuromast, were well correlated with changes in the initial response components. This was found in all six afferents investigated for both the rectified velocity (mean r^2 at position of the neuromast: 0.32±0.12 and 0.16±0.06 at the neighboring integration vector) and the vector angles (mean r^2 at position

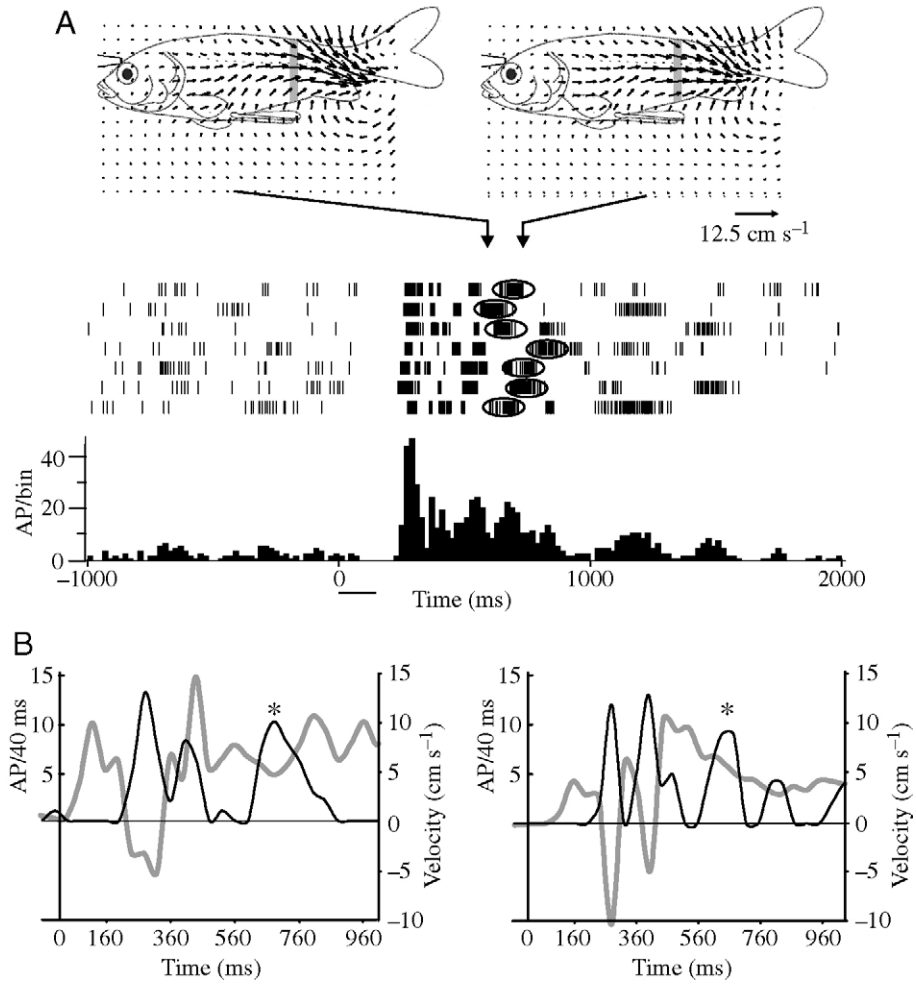

Fig. 12. (A) (Top) Averaged vector plots (n=7) based on particle motions caused by the vortex stimulus, (middle) raster plots of the responses to the vortex stimulus and (bottom) the peri-stimulus–time histograms (PSTH; bin width 20 ms) based on these raster plots. Zero indicates the time of valve opening. Averaged particle motions were recorded immediately before (left PIV image) and during (right PIV image) the non-reproducible bursts marked by the ellipses in the raster plot. (B) Discharge rates (black traces) and water velocities (gray traces) measured during the first (left graph) and seventh (right graph) trial shown in A. During the initial decrease in neural activity (90–190 ms after valve opening), water velocity was positive in both cases, i.e. water flow at the level of the neuromasts was from head to tail. During the following increase in neural activity, the direction of water flow reversed. No correlation between the occurrence of late bursts and water flow direction was apparent. Asterisks indicate the bursts marked with ellipses in A.

of the neuromast: 0.21±0.17 and 0.09±0.07 at the neighboring integration vector). Thus, the water motions measured at the position of the neuromast showed a higher correlation with the neural responses than the water motions measured at a more caudal location.

We also analyzed whether the late response component (late bursts) also correlated with flow patterns. In four cells, the late response component consisted of reproducible bursts. However, in none of these cells did neural activity predict flow direction (Wilcoxon test, n=4, $P \geqslant 0.2$; e.g. Fig. 11). Thus, in contrast to the initial and reproducible response components, there was no correlation between the occurrence of late and reproducible bursts and flow direction. However, an FFT analysis revealed that both discharge rates and water accelerations had prominent peaks at 3 and 8 Hz (see Fig. 11C). This indicates that the occurrence of late and reproducible bursts was partly due to alterations in local flow direction.

In most cells, the late response component did not show any reproducible bursts. In two of these cells, we investigated whether there was a correlation between flow direction and neural activity. In the two cells analyzed, changes in the initial response again correlated with a reversal in flow direction. However, changes in flow direction occurred neither at the beginning nor at the end of a late burst (a total of seven late bursts per cell were analyzed; Wilcoxon test, $P \geqslant 0.2$ performed on averaged vector plots; Fig. 12). Thus, in none of these cells did neural activity predict flow direction.

Discussion

The lateral line system of most fish consists of superficial neuromasts and of neuromasts embedded in canals. Flow-sensitive PLLN-afferents most likely innervate superficial neuromasts. PLLN-afferents that are flow insensitive most likely innervate canal neuromasts (Engelmann et al., 2000). In agreement with Engelmann et al. (2002), we found flow-sensitive and flow-insensitive PLLN-afferents. Although we especially searched for flow-insensitive (type II) afferents, the ratio between flow-sensitive and flow-insensitive afferents was 26:15. This ratio is in line with former studies (Engelmann et al., 2002) and the finding that goldfish have much more superficial than canal neuromasts (Puzdrowski, 1989).

In many studies, well-defined water motions, generated by a stationary sphere that vibrated with a constant amplitude and frequency, were used as a lateral line stimulus (Flock and

Wersäll, 1962b; Harris and van Bergeijk, 1962; Kroese et al., 1978; Bleckmann et al., 1989). To generate more complex (and presumably more natural) water motions, small objects passing the fish laterally were introduced as a stimulus source (Bleckmann and Zelick, 1993; Mogdans and Goenechea, 1999; Müller et al., 1996; Plachta et al., 2003). In the present study, a vortex that passed the fish laterally served as a hydrodynamic stimulus. Under natural conditions, many fish are exposed to vortex rings or individual vortices that occur behind stationary objects or in the wake of swimming fish (Bleckmann et al., 1991; Blickhan et al., 1992; Cheng and Chahine, 2001; Drucker and Lauder, 1999, 2000; Rosen, 1959). Behavioral sensitivity of fish to such vortices has been documented (Tou, 1991). For piscivorous fish, the detection of vortices may be of importance for prey detection and hydrodynamic trail following (Hanke et al., 2000; New et al., 2001). Catfish (Pohlmann et al., 2001, 2004) and seals (Dehnhardt et al., 2001) may use information preserved in vortices to track down prey. Thus, vortices are of biological significance.

Neural responses to vortices

Peripheral lateral line units of goldfish responded with fairly predictable discharges to the vortex stimulus. With four exceptions, the initial response patterns were monophasic, biphasic or triphasic. Monophasic responses consisted of one increase or decrease in neural activity that often was followed by a weak decrease or increase in discharge rate. However, the second change in neural activity did not match our threshold criteria. Biphasic responses consisted of an increase in ongoing activity followed by a decrease in discharge rate or *vice versa*. In triphasic responses, an additional reproducible change in neural activity occurred. Thus, the initial responses of goldfish lateral line afferents to the vortex stimulus compare well with the initial responses of many PLLN-afferents to an object passing the fish laterally (Mogdans and Bleckmann, 1998). With respect to the initial response component, different lateral line afferents may show a reversed temporal response pattern to a moving object or to a passing vortex. In addition, the initial reproducible response pattern of most PLLN-afferents reversed if the direction of object motion was reversed (Bleckmann and Zelick, 1993; Engelmann et al., 2003; Mogdans and Bleckmann, 1998). Most likely, these findings can be explained by the directionality of lateral line hair-cells (e.g. Flock and Wersäll, 1962a; Görner, 1963). Since lateral line neuromasts contain two populations of hair cells that are aligned in opposite directions, and since individual lateral line afferents innervate only hair cells of the same alignment, one expects that different afferents may respond in directly opposite ways to the same moving object stimulus. The antagonistic orientation of hair cells in the sensory epithelium of a lateral line neuromast also implies that the response patterns of lateral line afferents invert when flow direction reverses.

If stimulated with water motions caused by a moving object, lateral line units assumed to receive input from superficial neuromasts continued to fire unpredictable bursts of spikes after the object had passed the fish laterally (Bleckmann and Zelick, 1993; Engelmann et al., 2003; Mogdans and Bleckmann, 1998). Moving objects not only generated initial reproducible water motions but also late water oscillations that were less predictable. These late water oscillations most likely caused the late ill-defined response bursts (Mogdans and Bleckmann, 1998). Using our stimulus, many type I and type II PLLN-afferents continued to fire unpredictable bursts long after the vortex had passed the fish. Thus, both flow-sensitive and flow-insensitive afferents responded similar to the vortex stimulus.

Correlation of neural responses with PIV data

If one wants to correlate neural responses with the water motions that have caused these responses, a precise determination of the position of the neuromast is crucial. We did not attempt to determine the dorso-ventral position of the neuromast since the water motions caused by the vortex stimulus were fairly symmetrical across the dorso-ventral extent of the fish (e.g. Fig. 2). Therefore, the dorso-ventral position of the neuromast most likely had little influence on the afferent responses. However, with respect to the long axis of the fish, we precisely determined the position of the neuromast in 25 cases. In 12 of these cases, we compared the PIV data with the neural data of afferents whose receptive fields had been determined precisely off-line.

Our PIV measurements confirmed that the passing of the vortex stimulus from rostral to caudal caused either an E- or an I-response in a given afferent (see Figs 10, 11). This supports the assumption that, all else being equal, the temporal response pattern of an afferent depends on the orientation of the hair cells innervated by that afferent. For the initial reproducible response component, our PIV measurements show, in addition, that an inversion in flow direction caused an inversion in the temporal characteristics of the neural response. To our surprise, there was no or, at best, a weak correlation between the late ill-defined response component and the water motions recorded simultaneously. One possible explanation is that the distance between the laser sheet and the surface of the fish was >1 mm. Due to reflections of the laser sheet and the curvature of the fish, smaller distances were not possible. Since lateral line cupulae have a length of <1 mm (Teyke, 1990), we were unable to monitor the water motions in their immediate vicinity. Hence, we cannot rule out that the water motions responsible for the neural responses were not always identical with the particle motions measured in the light sheet. The lack of correlation between particle motions and the late response component may also be due to undetected minor alterations in water velocity and/or flow direction, i.e. changes exceeding the spatial and/or temporal (25 Hz) resolution of our PIV system.

One can expect that the neural response of primary lateral line afferents correlates well with the velocity and the direction of the water motions that impinge on a neuromast (e.g. Flock, 1962; Görner, 1963). However, if we record from central lateral line units, i.e. from lateral line units that may receive input from several neuromasts distributed across a larger part of the fish's body, this method may be very helpful in

uncovering the complex spatio-temporal flow patterns that may be necessary to drive some central units. Future experiments will show whether this prediction is correct.

This paper is dedicated to the memory of T. H. Bullock, one of the pioneers in sensory physiology and neurobiology. Ted Bullock had already suggested 20 years ago that we should use more natural and complex stimuli to study the lateral line. We gratefully acknowledge the help of C. Brücker in the generation of vortex rings. We would like to thank J. Mogdans, S. Kröther and S. Coombs for critically reading and commenting on an early draft of the manuscript. We are indebted to W. Hanke and M. Hofmann for technical help. The manuscript was improved by the comments of two anonymous reviewers. The experiments reported on in this paper comply with the current animal protection law of the Federal Republic of Germany ('Tierschutzgesetz'). This work was supported by a grant of the DFG (Bl-242/10-1).

References

Bleckmann, H. (1994). Reception of hydrodynamic stimuli in aquatic and semiaquatic animals. In *Progress in Zoology*, vol. 44 (ed. W. Rathmayer). Stuttgart, Jena, New York: Gustav Fischer.

Bleckmann, H. and Zelick, R. (1993). The responses of peripheral and central mechanosensory lateral line units of weakly electric fish to moving objects. *J. Comp. Physiol. A* **172**, 115-128.

Bleckmann, H., Weiss, O. and Bullock, T. H. (1989). Physiology of lateral line mechanoreceptive regions in the elasmobranch brain. *J. Comp. Physiol. A* **164**, 459-474.

Bleckmann, H., Breithaupt, T., Blickhan, R. and Tautz, J. (1991). The time course and frequency content of hydrodynamic events caused by moving fish, frogs, and crustaceans. *J. Comp. Physiol. A* **168**, 749-757.

Blickhan, R., Krick, C., Breithaupt, T., Zehren, D. and Nachtigall, W. (1992). Generation of a vortex-chain in the wake of a subundulatory swimmer. *Naturwissenschaften* **79**, 220-221.

Cheng, J. Y. and Chahine, G. L. (2001). Computational hydrodynamics of animal swimming: boundary element method and three-dimensional vortex wake structure. *Comp. Biochem. Physiol.* **131A**, 51-60.

Coombs, S., Hastings, M. and Finneran, J. (1996). Modeling and measuring lateral line excitation patterns to changing dipole source locations. *J. Comp. Physiol. A* **178**, 359-371.

Dehnhardt, G., Mauck, B., Hanke, W. and Bleckmann, H. (2001). Hydrodynamic trail-following in harbor seals (*Phoca vitulina*). *Science* **293**, 102-104.

Drucker, E. G. and Lauder, G. V. (1999). Locomotor forces on a swimming fish: three-dimensional vortex wake dynamics quantified using digital particle image velocimetry. *J. Exp. Biol.* **202**, 2393-2412.

Drucker, E. G. and Lauder, G. V. (2000). A hydrodynamic analysis of fish swimming speed: wake structure and locomotor force in slow and fast labriform swimmers. *J. Exp. Biol.* **203**, 2379-2393.

Engelmann, J., Hanke, W., Mogdans, J. and Bleckmann, H. (2000). Hydrodynamic stimuli and the fish lateral line. *Nature* **408**, 51-52.

Engelmann, J., Hanke, W. and Bleckmann, H. (2002). Lateral line reception in still- and running water. *J. Comp. Physiol. A* **188**, 513-526.

Engelmann, J., Kröther, S., Bleckmann, H. and Mogdans, J. (2003). Effects of running water on lateral line responses to moving objects. *Brain Behav. Evol.* **61**, 195-212.

Flock, A. and Wersäll, J. (1962a). A study of the orientation of the sensory hairs of the receptor cells in the lateral line organ of fish, with special reference to the function of the receptors. *J. Cell Biol.* **15**, 19-27.

Flock, A. and Wersäll, J. (1962b). Synaptic structures in the lateral line canal organ of the teleost fish Lota vulgaris. *J. Cell Biol.* **13**, 337-343.

Flock, A. and Duvall, A. J., 3rd (1965). The ultrastructure of the kinocilium of the sensory cells in the inner ear and lateral line organs. *J. Cell Biol.* **25**, 1-8.

Görner, P. (1963). Untersuchungen zur Morphologie und Elektrophysiologie des Seitenlinienorgans vom Krallenfrosch (*Xenopus laevis* Daudin). *Z. Vergl. Physiol.* **47**, 316-338.

Hanke, W. and Bleckmann, H. (2004). The hydrodynamic trails of Lepomis gibbosus (Centrarchidae), Colomesus psittacus (Tetraodontidae) and Thysochromis ansorgii (Cichlidae) investigated with scanning particle image velocimetry. *J. Exp. Biol.* **207**, 1585-1596.

Hanke, W., Brucker, C. and Bleckmann, H. (2000). The ageing of the low-frequency water disturbances caused by swimming goldfish and its possible relevance to prey detection. *J. Exp. Biol.* **203**, 1193-1200.

Harris, G. G. and van Bergeijk, J. D. (1962). Evidence that the lateral line organ responds to near-field displacements of sound sources in water. *J. Acoust. Soc. Am.* **34**, 1831-1841.

Kalmijn, A. J. (1988). Hydrodynamic and acoustic field detection. In *Sensory Biology of Aquatic Animals* (ed. J. Atema, R. R. Fay, A. N. Popper and W. S. Tavolga), pp. 151-186. New York: Springer.

Kroese, A. B., Van der Zalm, J. M. and Van den Bercken, J. (1978). Frequency response of the lateral-line organ of *Xenopus laevis*. *Pflügers Arch.* **375**, 167-175.

Liao, J. C., Beal, D. N., Lauder, G. V. and Triantafyllou, M. S. (2003). Fish exploiting vortices decrease muscle activity. *Science* **302**, 1566-1569.

Linden, P. F. and Turner, J. S. (2004). 'Optimal' vortex rings and aquatic propulsion mechanisms. *Proc. R. Soc. Lond. B Biol. Sci.* **271**, 647-653.

Mogdans, J. and Bleckmann, H. (1998). Responses of the goldfish trunk lateral line to moving objects. *J. Comp. Physiol. A* **182**, 659-676.

Mogdans, J. and Goenechea, L. (1999). Responses of medullary lateral line units in the goldfish, *Carassius auratus*, to sinusoidal and complex wave stimuli. *Zoology* **102**, 227-237.

Müller, H. M., Fleck, A. and Bleckmann, H. (1996). The responses of central octavolateralis cells to moving sources. *J. Comp. Physiol. A* **179**, 455-471.

Münz, H. (1979). Morphology and innervation of the lateral line system of *Sarotherodon niloticus* L. (Cichlidae, Teleostei). *Zoomorphololgy* **93**, 73-86.

New, J. G., Alborg Fewkes, L. and Khan, A. N. (2001). Strike feeding behavior in the muskellunge, *Esox masquinongy*: contributions of the lateral line and visual sensory systems. *J. Exp. Biol.* **204**, 1207-1221.

Plachta, D. T., Hanke, W. and Bleckmann, H. (2003). A hydrodynamic topographic map in the midbrain of goldfish *Carassius auratus*. *J. Exp. Biol.* **206**, 3479-3486.

Pohlmann, K., Grasso, F. W. and Breithaupt, T. (2001). Tracking wakes: the nocturnal predatory strategy of piscivorous catfish. *Proc. Natl. Acad. Sci. USA* **98**, 7371-7374.

Pohlmann, K., Atema, J. and Breithaupt, T. (2004). The importance of the lateral line in nocturnal predation of piscivorous catfish. *J. Exp. Biol.* **207**, 2971-2978.

Puzdrowski, R. L. (1989). Peripheral distribution and central projections of the lateral-line nerves in goldfish, *Carassius auratus*. *Brain Behav. Evol.* **34**, 110-131.

Rosen, M. W. (1959). *Waterflow About a Swimming Fish*. China Lake, CA: US Naval Ordnance Test Station Publications.

Sutterlin, A. M. and Waddy, S. (1975). Possible role of the posterior lateral line in obstacle entrainment by brook trout (*Salvelinus fontinalis*). *J. Fish. Res. Bd. Can.* **32**, 2441-2446.

Teyke, T. (1990). Morphological differences in neuromasts of the blind cave fish *Astyanax hubbsi* and the sighted river fish *Astyanax mexicanus*. *Brain Behav. Evol.* **35**, 23-30.

Tou, S. K. W. (1991). A statistical and experimental study on fish response subject to vortex ring motion. *J. Environ. Sci. Health A* **26**, 755-775.

Vogel, S. (1984). *Life in Moving Fluids. The Physical Biology of Flow*. Second edn. Princeton: Academic Press.